Examining ^{239}Pu and ^{240}Pu Nuclear Resonance Fluorescence Measurements on Spent Fuel for Nuclear Safeguards

Brian J. Quiter,* Thibault Laplace,† and Bernhard A. Ludewigt‡
Lawrence Berkeley National Laboratory, Berkeley, CA 94720

In nuclear resonance fluorescence (NRF) measurements, resonances are excited by an external photon beam leading to the emission of gamma rays with specific energies that are characteristic of the emitting isotope. NRF promises the unique capability of directly quantifying the concentration of a specific isotope in spent fuel without the need for unfolding the combined responses of several fissile isotopes as is required many in other measurement techniques. Despite this promise, the implementation of a practical measurement system is quite difficult because of limitations in photon source and gamma-ray detector technologies. These limitations, combined with the low concentration in ^{239}Pu in spent fuel and its relatively weak NRF resonances would make a direct measurement of ^{239}Pu content using available technology very time-consuming. The effects of improved photon source technology as well as alternative detector types will be discussed in terms of the gain in statistical precision that can be achieved for a given measurement duration. Because of the difficulty in measuring ^{239}Pu via NRF, the strengths and energies of ^{240}Pu resonance states have recently been experimentally measured. As expected, significantly stronger resonances were observed at excitation energies similar to those of ^{239}Pu. The impact of these stronger resonances on nuclear safeguards measurements will be discussed using a combination of MCNPX simulations that have been experimentally checked, and analytical model-based predictions. The modeling suggests that ^{240}Pu will generally be less difficult to quantify via NRF than ^{239}Pu because of these larger cross sections, despite generally lower concentration in spent fuel. Therefore the time-scales, photon source and detector systems requirements for high-accuracy NRF measurements of ^{240}Pu in spent fuel will also be examined.

*bjquiter@lbl.gov
†tlaplace@lbl.gov
‡Bernhard_Ludewigt@lbl.gov

I. INTRODUCTION

Nuclear resonance fluorescence (NRF) has been identified as a technology that is capable of directly measuring concentrations of specific isotopes within large areal density targets. Because of this, the phenomenon has received attention for potential uses in problems such as measuring plutonium isotopes in spent fuel and identifying nuclear weapons in cargo [1–3]. However, NRF-based interrogation schemes are not without drawbacks. The resonances of the actinide isotopes, ^{235}U and ^{239}Pu, were measured and the strengths of the resonances were relatively weak. The implications of these resonances strengths were discussed in previous INMM papers, which indicated that very strong photon sources and large detector arrays would be necessary to make a practical measurement of the ^{239}Pu content in spent nuclear fuel [4, 5]. Development of more intense narrow band photon sources has continued at various institutions, [6, 7] alternative NRF γ ray detection techniques have been proposed [8], and the NRF response of ^{240}Pu has been measured [9]. This paper provides an update to estimates of the measurement requirements for NRF measurement of Pu in spent fuel, given these advances.

Section II summarizes NRF measurement techniques in the context of spent nuclear fuel, summarizes the results of the first ^{240}Pu NRF experiment, and provides some context for application of these results towards non-destructive assay measurements using NRF. Section III presents the results of Monte Carlo simulations of ^{240}Pu measurements in spent fuel using pulsed quasi-monoenergetic photon sources and HPGe detectors and compares these measurements to similar ^{239}Pu measurements, such as those previously described. Lastly, the use of calorimetric detectors to measure ^{239}Pu or ^{240}Pu in spent fuel was considered and is discussed in Section IV. This discussion indicates that calorimetric detectors could be very effective, given the present directions of quasi-monoenergetic photon source development.

II. NRF MEASUREMENT TECHNIQUES

Techniques used to perform NRF measurements involve a photon source that excites resonances and a measurement system that either directly measures NRF γ ray emissions, or a downstream system that measures the reduced spectral intensity of photons that have been resonantly absorbed. The two types are referred to as backscatter and transmission measurements, respectively. Because γ-ray detector resolutions tend to be significantly wider than the width of NRF resonances, direct measurement of NRF γ ray emission tends to only be practical in select cases, such as when the measurement material has a large fraction of the isotope being measured, which is never the case for measurement of Pu in spent fuel; or when the photon beam that causes resonant excitation is sufficiently narrow that it effectively defines the energy resolution of the overall NRF measurement system, rather than the γ-ray detector. Even in the latter, ideal case, direct measurement of NRF γ ray emissions remains challenging due to the radioactivity of the spent fuel. This was discussed in more detail in previous reports[3, 4].

Transmission measurements have the key advantage that the radiation detectors may be well-shielded from the spent fuel activity. This is because down-beam of the assayed assembly, a sheet of a specific isotope or isotopic mixture, referred to herein as a transmission detector foil (TD), may be placed in the beam with radiation detectors oriented to view photons scattered from it yet heavily shielded in other directions. Because the TD may be comprised essentially of a single isotope, NRF γ rays may represent an appreciable fraction of a measured signal in this configuration. However, because it is the reduction in the rate at which the TD undergoes NRF that is indicative of the areal density, ρx, of the corresponding isotope in the measured assembly, the uncertainty in the isotopic content in the assembly is inversely proportional to the derivative of the function relating the NRF rate in the TD to the areal density of the TD isotope in the target. This derivative is referred to herein as α. The process of using a TD to perform transmission NRF measurements has been previously described in some detail for ^{239}Pu[5].

The fractional statistical uncertainty in areal density associated with a transmission measurement is given by

$$\frac{\sigma_{\rho x}}{\rho x} = \frac{1}{\alpha \rho x}\sqrt{\frac{1+2/\xi}{C_{\mathrm{NRF}}}} \tag{1}$$

where C_{NRF} is the number of counts attributed to NRF, and ξ is the corresponding signal-to-background ratio. The quantity, α, is obtained by evaluating the absolute value of the derivative of the *effective attenuation* curve (Figure 2(a)) for a particular resonance at the corresponding areal density.

Although Equation 1 is not related in a simple way to the strength of a measured resonance (i.e. $\int \sigma dE$), the terms α, C_{NRF}, and ξ are all proportional to $\int \sigma dE$. This results in a strong relation between the strength of the resonance and its effectiveness for quantifying the areal density of the corresponding isotope in a target.

The ^{240}Pu NRF response was measured in 2011 using a bremsstrahlung photon source with 3 MeV endpoint energy. The results of this measurement have recently been submitted for publication [9]. As anticipated, the largest ^{240}Pu resonances are comparable to ^{238}U in strength and are at similar excitation energies ($\sim$ 2.5 MeV)[10]. The largest

observed resonance, at $E = 2.433$ MeV, appears to have been previously observed in NRF measurements of weapons-grade Pu, and was tentatively assigned as a ^{239}Pu transition, rather than a ^{240}Pu transition [11]. A result of this finding is that ^{240}Pu has resonances that are ~ 5.5 times stronger than the ^{239}Pu resonances. This is an important finding for NRF measurements because the statistical uncertainty associated with a transmission NRF measurement scales non-linearly with the strength of the resonance(s) measured.

Using the results of the ^{240}Pu NRF measurement, the effects of ^{240}Pu TD thicknesses may be compared to ^{239}Pu filter thicknesses. In general, the use of a thicker TD produces more NRF, which improves the rate at which NRF counts are observed, but it also results in more non-resonantly back-scattered radiation, which worsens ξ. Also the use of the thinnest plutonium TD practical is preferable for materials control reasons. The effective relative efficiencies of transmission detectors as functions of Pu TD thicknesses a shown for the ^{240}Pu resonance at 2433 keV and the 2143 keV ^{239}Pu resonance in Figure 1. Weaker ^{239}Pu resonances motivate the use of a thicker TD and a 1-cm-thick ^{239}Pu TD was assumed for ^{239}Pu measurements as opposed to a 4-mm-thick ^{240}Pu TD for ^{240}Pu measurements. However, neither filter thickness has been subjected to optimization.

Functional relationships between expected NRF rates in a ^{240}Pu TD were calculated as a function of areal density of ^{240}Pu within the assay target for each ^{240}Pu NRF state. Example relations are shown in Figure 2(a) for states at 2433, 2464 and 2566 keV. The integrated strength of these states are 104, 43 and 69 eV·b, respectively. This nearly spans the range of resonances strengths that have been observed for ^{240}Pu, although weaker states are likely present, but went unobserved in the measurement.

The parameter, α in Equation 1 denotes the magnitude of the slope of the functions shown in Figure 2(a). Since the fractional uncertainty of the areal density of the NRF isotope in the spent fuel assembly (i.e. ^{240}Pu) is inversely proportional to α, it is instructive to examine this function in more detail. The functional relation between α and the areal density of ^{240}Pu in an assembly is shown (again, for a 4-mm-thick TD) in Figure 2(b) for the three ^{240}Pu resonances discussed previously. For ^{240}Pu areal densities typical of spent fuel (i.e., ~ 0.3 g/cm^2), the strongest resonance will produce the smallest transmission measurement uncertainty. The value of α does decrease with increasing ρx, which effectively limits the dynamic range over which a single resonance can effectively be used to measure a target. For ^{240}Pu, when ρx exceeds 13.5 g/cm^2, the slope of the attenuation curve for the 2433 keV resonance becomes smaller than that for the 2566 keV resonance. Likewise, at $\rho x = 20.8$ g/cm^2, the 2464 keV resonance has the largest values of α. This implies that smaller resonances become more effective for measuring composition at very high areal densities, thereby dramatically increasing the overall dynamic range of transmission NRF measurements. While it is not anticipated that this regime would ever be important for spent nuclear fuel, in applications such as nuclear weapons verification measurements, smaller resonances may prove more practical to measure.

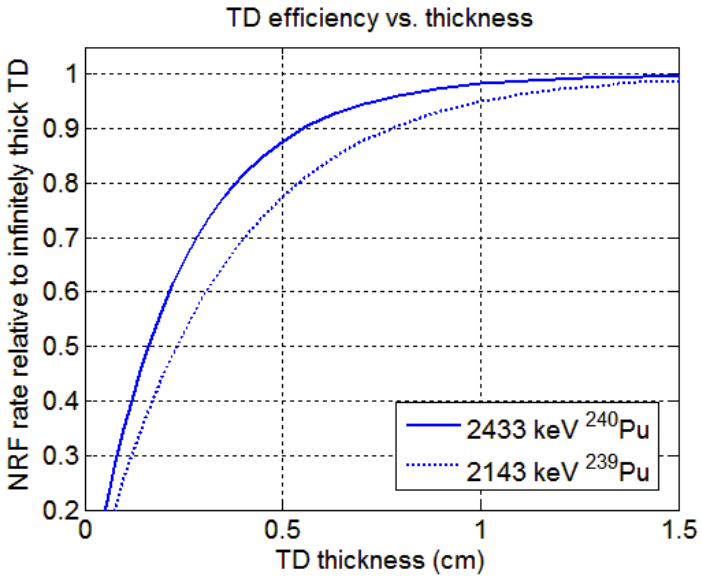

FIG. 1: Calculated relative TD efficiencies versus thickness for the largest observed ^{239}Pu and ^{240}Pu resonances.

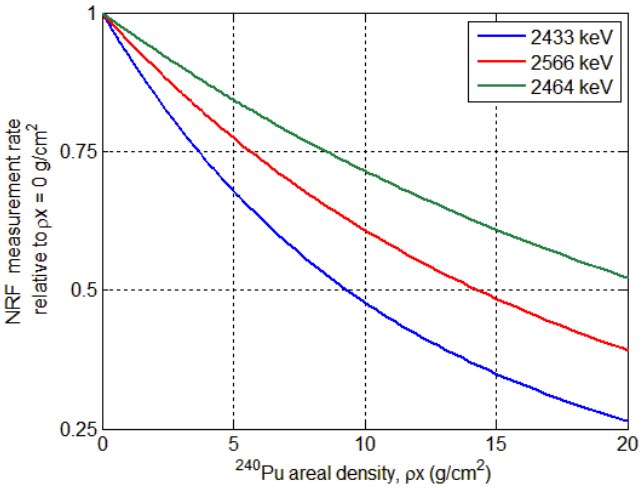

(a)Relative resonant attenuation versus ^{240}Pu areal density for 4-mm-thick TD.

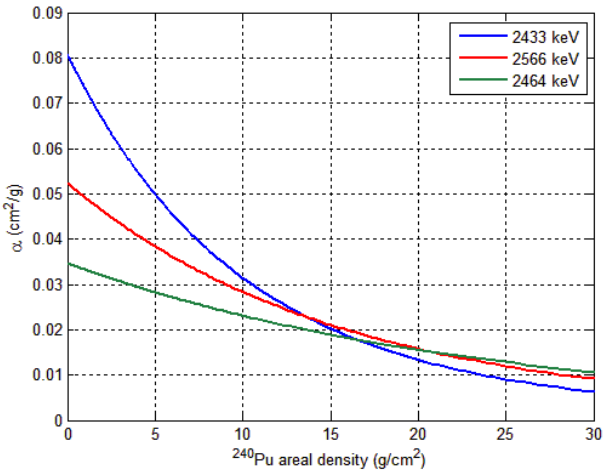

(b)Differentiated resonant attenuation function, $\alpha(\rho x)$, for various ^{240}Pu resonances.

FIG. 2:

III. ^{240}PU MEASUREMENTS WITH QUASI-MONOENERGETIC PHOTON SOURCES

In spent fuel, ^{240}Pu concentration increases with exposure, before reaching a plateau near 0.25% of the total isotopic composition in typical spent fuel (compared to 0.45% for ^{239}Pu). The corresponding areal density depends upon the path photons take as they traverse spent fuel. Different irradiation geometries have been considered, (see Figures 3(a) and 3(b)), corresponding to areal densities of 0.21 and 0.37 g/cm^2 for the geometries labeled A and B, respectively. A fuel assembly that is measured while submerged in H_2O has identical Pu areal densities, and this possibility is also examined in the following.

Compared to ^{239}Pu, the larger ^{240}Pu resonances result in larger values of α and yield higher NRF count rates; both of these facts result in smaller statistical uncertainties for ^{240}Pu than for ^{239}Pu in similar transmission measurements. Although ^{240}Pu does result in more resonant attenuation, relative to ^{239}Pu in spent fuel, the increase is not so much as to result in a reduced sensitivity of the transmission measurement.

To quantify the reduction in uncertainty associated with Pu in spent fuel by measuring ^{240}Pu, rather than ^{239}Pu, MCNPX simulations were performed to determine the resonant and non-resonant count rates in various detector types that are well-shielded and positioned to view a TD positioned down-stream from a spent fuel assembly that is irradiated with 2433 keV photons (corresponding to the largest ^{240}Pu resonance)[12–15]. These simulations are analogous to simulations previous described for ^{239}Pu [5]. The simulations produce count rates as functions of energy for resonant and non-resonant source photons for detectors with various filter thicknesses that view an isotopically pure plutonium TD. The count rates calculated for resonant and non-resonant photons are subsequently weighted according to an assumed beam energy distribution and summed to produce predicted detector responses. For HPGe detectors, it is assumed that the signal attributed to NRF is only the full energy peak from NRF γ rays, and the primariy background is due to elastic non-resonant scatter of beam photons in the TD.

A summary of the modeling is shown in Table I for a single 100% relative efficiency germanium detector, positioned behind a Pb filter, viewing a ^{240}Pu TD from a distance of 20 cm. The NRF count rate is determined assuming no resonant attenuation within the assembly (i.e. the ordinate value in Figure 2(a) is unity, and reductions in NRF count rates are subsequently determined by referring to Figure 2(a)). Photon detection probabilities for resonant and non-resonant source photons are tabulated, $P_{\rm res}$, and $P_{\rm NR}$, respectively; as well as the probability for measuring full-energy NRF γ rays given a resonant source photon, $C_{\rm NRF}$; and lastly, the probability for measurement of a full-energy elastic scatter photon given a non-resonant source photon, $C_{\rm ES}$. The latter is the primary source of background for energy-resolving detectors.

It is evident in Table I that increasing filter thickness, x_f, reduces the rate at which non-resonant photons are measured, $P_{\rm NR}$, more rapidly than the corresponding rate for resonant photons, $P_{\rm res}$. This is the main reason that filters are effective, although their effectiveness is reduced as their thickness increases. The rotated geometry was selected to achieve a more uniform path length through the assembly when the assembly is translated, and because of shorter paths through the fuel, results in approximately 10 times the overall count rate, relative to geometry A. However, the rotated geometry also results in more water in the photon path when the assembly is submerged. This

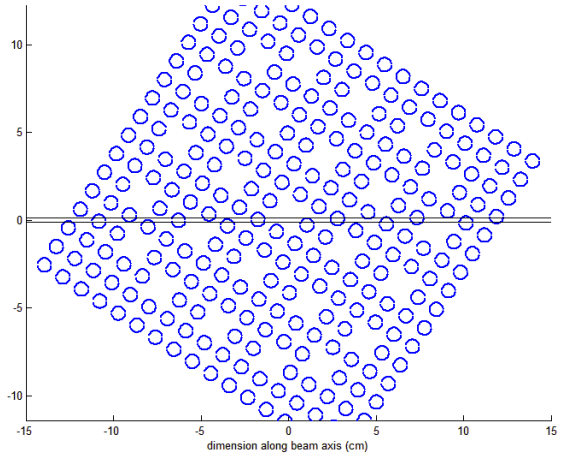

(a)Geometry A, beam transmitted through assembly rotated 33°.

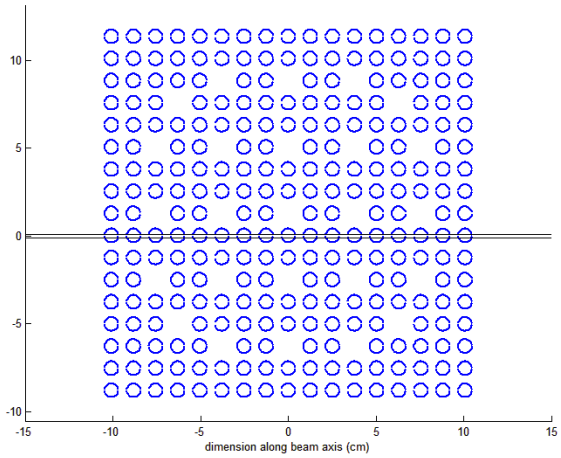

(b)Geometry B, beam transmitted through row of assembly with 17 pins.

FIG. 3: Pin locations and beam trajectory for simulated geometries. Geometries were also simulated with assembly in and out of water. The extent of water in the models did not extend far beyond the assembly dimension.

TABLE I: Results of simulations of transmission measurements for 2433 keV photons used to measure ^{240}Pu in a spent fuel assembly for geometries A and B in (denoted by 'w') and out of water.

geometry	x_f (cm)	$P_{\rm res}$	$P_{\rm NR}$	$C_{\rm NRF}$	$C_{\rm ES}$
A	1.3	1.9×10^{-5}	2.6×10^{-6}	2.0×10^{-6}	3.1×10^{-11}
A	2.5	1.1×10^{-5}	5.4×10^{-7}	1.1×10^{-6}	1.7×10^{-11}
A	5.0	4.1×10^{-6}	5.9×10^{-8}	3.3×10^{-7}	5.0×10^{-13}
Aw	1.3	9.8×10^{-6}	1.4×10^{-6}	1.0×10^{-6}	1.6×10^{-11}
Aw	2.5	5.6×10^{-6}	2.8×10^{-7}	5.6×10^{-6}	8.6×10^{-12}
Aw	5.0	2.1×10^{-6}	3.0×10^{-8}	1.7×10^{-7}	2.6×10^{-12}
B	1.3	1.8×10^{-6}	3.1×10^{-7}	1.9×10^{-7}	3.5×10^{-12}
B	2.5	1.0×10^{-6}	6.7×10^{-8}	1.0×10^{-7}	1.9×10^{-12}
B	5.0	3.9×10^{-7}	7.6×10^{-9}	3.0×10^{-8}	5.7×10^{-13}
Bw	1.3	1.4×10^{-6}	2.3×10^{-7}	1.4×10^{-7}	2.6×10^{-12}
Bw	2.5	7.8×10^{-7}	4.7×10^{-8}	7.7×10^{-8}	1.4×10^{-12}
Bw	5.0	2.9×10^{-7}	4.9×10^{-9}	2.3×10^{-8}	4.2×10^{-13}

causes a factor of two further reduction in count rates, as opposed to a 30% reduction for the un-rotated geometry. The relative importance of these factors depends on the photon source and detector constraints, which will be discussed later.

The results shown in Table I are combined for select photon source distributions, assuming each has a Gaussian energy profile with standard deviation energy dispersion, σ_S. The possibility of non-resonant photons down-scattering to the resonant energy (called *notch-refill*) is neglected. This can result in lower values of α than those reported here, but has been estimated elsewhere for ^{238}U resonances of similar strength as a ∼5% effect for bremsstrahluhng beams [16], and it has been predicted to be an even smaller effect for QM beams[2]. Ideally, the intensitiy and repetition rate of the photon source would not be limiting factors. In this case, thick filters (5-8 cm) and long paths through assemblies are preferable and measurement of an assembly that is submerged in water during the measurement is unproblematic. A summary of measurement parameters for a single HPGe detector shielded with a 5 cm Pb filter is shown in Table II for measurement of an assembly submerged in water and in geometry B (ρx = 0.373 cm^2/g),

TABLE II: Measurement parameters for a measurement of ^{240}Pu content in a spent fuel assembly submerged in water, in Geometry B for various photon source energy dispersions, σ_S, using a single HPGe detector positioned behind a 5-cm-thick Pb filter. The probability of photon detection per beam pulse is held at 0.01, which defines the beam pulse intensity and the overall beam intensity, I_S, assuming a 1 MHz beam.

σ_S (keV)	ξ	I_S (1/s)	f_S	C_{NRF} (1/s)	$t_{3\%}$ (hr)
0.1	743	7.1×10^{5}	3.2×10^{-2}	1105	0.34
0.5	145	1.5×10^{6}	6.4×10^{-3}	440	0.8
1	72	1.7×10^{6}	3.2×10^{-3}	255	1.4
5	38	2.0×10^{6}	6.4×10^{-4}	58	6.54
10	38	2.0×10^{6}	3.2×10^{-4}	30	12.7
30	38	2.0×10^{6}	1.1×10^{-4}	10	37.5

and a photon beam whose total intensity is un-constrained except that the beam has been assumed to be pulsed at a frequency of 2 MHz and the total count probability per pulse, P_{det}, is set to 0.01. This results in a total count rate in the detector of 20 kHz and a probability for coincident pulse summing of 1×10^{-4}.

The parameters shown in the columns of Table II are the following: ξ is the strength of the NRF signal, relative to the elastic scatter background; I_S is the number of emitted source photons per shot that are directed towards the TD; f_S is the fraction of these source photons that are effectively resonant[1]; C_{NRF} is the rate of NRF full energy depositions; and $t_{3\%}$ is the live-time necessary for a single HPGe detector to accure a 3% statistical uncertainty in the quantity of ^{240}Pu traversed in the assembly by the beam. It is assumed that more detectors would proportionally reduce measurement time; i.e., if the hemisphere subtending all back-angles for photons scattered in the TD were covered by 50 similar HPGe detectors, the measurement time would correspondingly be reduced by a factor of 50.

Table II indicates that with very strong beams, rapidly pulsed (or continuous) beams, measurement of the ^{240}Pu content in spent fuel to a few percent uncertainty could be achieved in hours, or faster, if multiple detectors are used. The most important parameter for such a measurement, in the limit of very strong photon sources, is the energy dispersion of the beam, σ_S. As this decreases, larger fractions of the source photons are resonant and it is only these photons that actually provide information. The values of σ_S currently being pursued are in the 1-5 keV range, so in this regard the parameters in this table indicate that NRF measurements of ^{240}Pu content in spent fuel could be very practical.

However, the values in Table II may also be considered the best-case values for a continuous or quasi-continuous beam[2]. Photon sources that are currently being developed appear more likely to be have repetition rates closer to 100-1,000 Hz, rather than 2 MHz. Keeping other parameters equal, would result in proportionally longer measurement times. As mentioned previously, up to 50 HPGe detectors could be accommodated in the simulated geometry, but if the detectors were positioned further from the TD, more detectors could be accommodated, and the count rate and P_{det} would be reduced. This would enable further increases in I_S to achieve the same count rate per detector, however increasing the quantity of detectors used is potentially very costly.

The data in Table II are also compared to the results of an analysis of a similar measurement of ^{239}Pu using the 2143 keV resonance. Although the ^{239}Pu areal density is nearly twice that of ^{240}Pu and a thicker filter was simulated, the measurement time to achieve a particular fractional uncertainty (i.e. $t_{3\%}$) was 40 to 100 times longer than for the ^{240}Pu measurement[3]. The range in increased relative measurement times is due to the fact that ξ is dependent on beam energy dispersion, and in the case that σ_S is small, ξ is suffiecently high that it may be neglected for both ^{239}Pu and ^{240}Pu in Equation 1. Conversely, as σ_S increases to near or above 3 keV, ξ becomes quite small for ^{239}Pu, which lessens the relative statistical values of each ^{239}Pu NRF count. These results, along with the fact that ^{240}Pu may be more convienent to use as a TD (from a perspective that it is less useful for weapons) are strong reasons to use ^{240}Pu to measure Pu in spent fuel.

---

[1] Defined in the simulations as within ± 4 eV of the resonance centroid.

[2] Although with values of ξ as high as they are here, it could be practical to reduce the detector resolution and measure at a higher count rate; although this would need to be accomplished with higher beam repetition rates, rather than higher intensity pulses.

[3] The measurement times given in reference [5] assumed no filter and a weaker source. The comparison made here assumed the same filter thickness (5 cm) and $P_{det} = 0.01$.

IV. CALORIMETRIC DETECTORS

The previous section indicated that quasi-monoenergetic source development will initially result in sources that, while very intense, will only have ∼Hz to ∼kHz repetition rates, rather than MHz or faster sources. As stated in the previous section, repetition rates below ∼MHz levels proportionally increase measurement times for measurement systems that employ typical HPGe detectors because coicident summing of pulses must be avoided. Alternatively, one could use a calorimetric detector, which does not measure individual photons, but instead is sensitive to the total energy deposition in the detector. This was initially proposed by Hall et al[8]. This type of detector would not be constrained by instantaneous count rates and could subtend a very large solid angle, potentially ∼2π, at a reasonable cost.

Calorimetric detectors rely on two phenomena: resonant photons are more likely than non-resonant photons at nearby energies to be backscattered, and the energies of backscattered resonant photons are higher, on average than the energies backscattered by non-resonant photons. As a result of these phenomena, NRF transmission measurement systems that use calorimetric detectors have advantages that may outweigh the disadvantage incurred by losing energy resolution. To illustrate the effect of a calorimetric detector, Figure 4 shows energy deposition spectra for a hemispherical NaI shell that is 40 cm thick, set behind a 1-cm-thick tantalum filter, and subtending nearly the entire 2π backwards hemisphere (except a 1-cm-diameter beam hole) of a 4-mm-thick ^{240}Pu TD from the simulation of 8-eV-wide uniform beams of resonant and non-resonant energy photons in geometry B with the assembly submerged in water. Clearly, significantly more counts and higher average energies result from the resonant energy photons. However, realistically broader energy dispersions of photon beams cause many times more non-resonant than resonant photons source photons, effectively lowering the resonant source photon energy deposition spectrum, relative to the non-resonant spectrum.

Whereas for energy-resolving detectors, increasing filter thickness improves the statistical value of the detected photons, it was observed that for calorimetric detectors there is an optimal filter thickness, whose dimension depends on the beam energy dispersion. These thicknesses, x_f(opt); the calorimetric signal due to resonant-energy photons, relative to that for non-resonant photons, ξ_C; the resonant and non-resonant photon measurement rates, $R_{\rm res}$ and $R_{\rm NR}$, respectively; and the time to obtain 3% statistical uncertainty, $t_{3\%}$, from a calorimetric measurement of ^{240}Pu in spent fuel assembly (i.e. geometry B, submerged in water), using a 1 kHz pulsed beam with 3×10^7 photons per pulse are shown in Table III. Two geometries are tabulted, the assembly in geometry B submerged in water, with 0.37 g/cm^2 of ^{240}Pu, and the assembly in geometry A in vacuum, with $\rho x = 0.21$ g/cm^2.

The most striking results shown in Table III is that the values of $t_{3\%}$ appear much lower than in Table II. However, in the latter, $t_{3\%}$ is only for a single detector rather than for a geometry in which the entire backward hemisphere is subtended by detectors. A more fair comparison would be to divded the values of $t_{3\%}$ in Table II by 50, at which point, $t_{3\%}$ is comparable between the two geometries for lower beam energy dispersions and becomes much larger

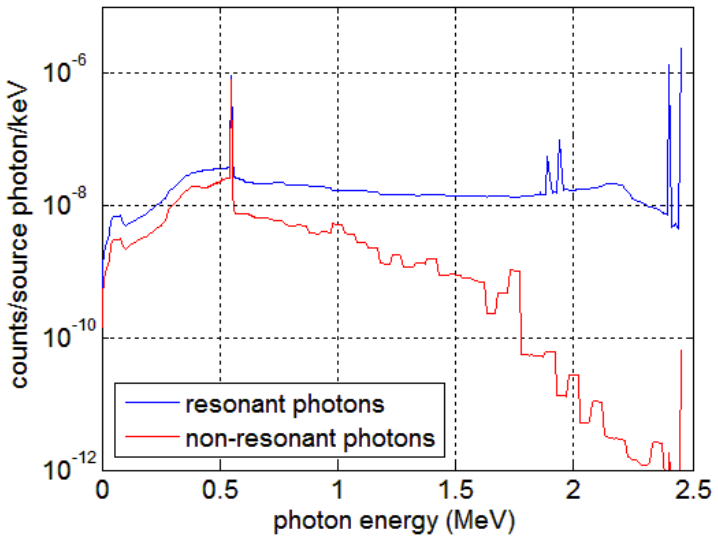

FIG. 4: Calculated energy deposition spectra per resonant and non-resonant photon for a calorimetric detector viewing a ^{240}Pu TD with a 10-mm-thick Ta filter.

TABLE III: Measurement parameters for a calorimetric measurement of ^{240}Pu content in a spent fuel assembly in two differing geometries for various photon source energy dispersions, σ_S and a 3×10^{10} photons/s source.

	geometry B, in water					geometry A, no water				
σ_S (keV)	x_f(opt) (mm)	ξ_C	$R_{\rm res}$ (1/s)	$R_{\rm NR}$ (1/s)	$t_{3\%}$ (hr)	x_f(opt) (mm)	ξ_C	$R_{\rm res}$ (1/s)	$R_{\rm NR}$ (1/s)	$t_{3\%}$ (hr)
0.1	11	5.7×10^{-1}	6.3×10^{4}	3.2×10^{5}	2.4×10^{-2}	11	6.6×10^{-1}	8.7×10^{5}	3.9×10^{6}	5.0×10^{-3}
0.5	23.1	2.7×10^{-1}	6.2×10^{3}	5.8×10^{4}	4.7×10^{-1}	22.5	3.1×10^{-1}	3.7×10^{4}	7.3×10^{5}	9.3×10^{-2}
1	25.3	1.6×10^{-1}	2.6×10^{3}	4.2×10^{4}	1.9×10^{0}	24.8	1.8×10^{-1}	3.7×10^{4}	5.2×10^{5}	3.6×10^{-1}
5	27.8	3.6×10^{-2}	4.7×10^{2}	3.1×10^{4}	4.1×10^{1}	27.5	4.3×10^{-2}	6.7×10^{2}	3.8×10^{5}	7.9×10^{0}
10	27.8	1.8×10^{-2}	2.4×10^{2}	3.1×10^{4}	1.6×10^{2}	27.9	2.2×10^{-2}	3.3×10^{3}	3.6×10^{5}	3.1×10^{1}
30	27.9	5.7×10^{-3}	7.8×10^{1}	3.1×10^{4}	1.5×10^{3}	28.2	7.3×10^{-3}	1.1×10^{3}	3.5×10^{5}	2.8×10^{2}

TABLE IV: Measurement parameters for a calorimetric measurement of ^{239}Pu content in a spent fuel assembly out of water, in Geometry A for various photon source energy dispersions, σ_S and a 3×10^{10} photons/s source.

σ_S (keV)	x_f(opt) (mm)	ξ_C	$R_{\rm res}$ (1/s)	$t_{3\%}$ (hr)
0.1	18	3.0×10^{-1}	1.6×10^{5}	1.1×10^{0}
0.5	22	7.8×10^{-2}	2.5×10^{4}	2.4×10^{1}
1	22.5	4.0×10^{-2}	1.2×10^{4}	9.6×10^{1}
5	23	8.3×10^{-3}	2.3×10^{3}	2.3×10^{3}
10	23	4.2×10^{-3}	1.1×10^{3}	9.4×10^{3}
30	23	1.4×10^{-3}	3.8×10^{2}	8.4×10^{4}

for calorimetric detectors and with larger beam dispersions. The importance of the energy dispersion of the source beam is discussed in the following. Very narrow beams cause a large fraction of the photons that interact in the detector to be due to NRF. As the beam dispersion widens, optimal filter thicknesses increase to compensate for a loss of resolution since non-resonant photons tend to backscatter with lower energy (on average) and are therefore more likely to be attenuated in the filter Increased filter thicknesses also result in lower count rates overall. This slows the accrual of counting statistics, resulting in longer counting times. As such, intense narrow bandwidth sources are critical for the application of calorimetric detectors in making NRF measurements.

Measurement of the ^{239}Pu content in spent fuel using a 2143 keV beam and a calorimetric detector has also been simulated. The results of a measurement for various source energy dispersions, using 3×10^{10} photons/s in geometry A and an assembly removed from water are shown in Table IV. The strong relation between $t_{3\%}$ and σ_S continues, however because the ^{239}Pu signal is weaker than that of ^{240}Pu, the predicted measurement times for ^{239}Pu are significantly longer.

V. CONCLUSIONS

Quasi-monoenergetic laser-Compton photon sources based on X-band linear accelerators and based on laser wake-field accelerators both appear to be capable of producing 10^7 to 10^8 photons per shot, with σ_S values in the keV range, and repetition rates in between 10's of Hz and kHz in the near future. Previous reports have indicated that such sources, even if continuous rather than pulsed, would not be sufficiently intense to make ^{239}Pu measurements in spent fuel assemblies using NRF practical. However, with the observation of significantly stronger ^{240}Pu resonances and because measurement times do not scale linearly with resonance strength, these photon sources could be practical for measuring ^{240}Pu with an array of HPGe detectors. Particularly, the time necessary to make a 3% statistical uncertainty measurement of ^{240}Pu in spent fuel is reduced by a factor of up to 32, relative to a similar measurement of ^{239}Pu in spent fuel using HPGe detectors.

Also, while the pulsed nature of beams being developed would cause count rate limitations for HPGe detectors that would necessitate source beams being used in NRF systems that are lower in per-pulse intensity than is expected to be developed, calorimetric detector types do not have these rate constraints. Therefore, very intense, pulse beams with narrow energy dispersions could potentially be very effective for ^{240}Pu measurements in spent fuel. Interestingly, the relative strength of the resonance that will be used to measure plutonium concentrations in fuel assemblies is

even more important for calorimetric detector types. Therefore, the significance of the recent observation of ^{240}Pu resonances further motivations the application of calorimetric detectors and the development of narrow-band photon sources.

Acknowledgments

This work was supported by the Offices of Proliferation Detection and Nonproliferation & International Security of the National Nuclear Security Administration, US Department of Energy under Contract No. DE-AC02-05CH11231.

[1] W. Bertozzi and R.J. Ledoux, "Nuclear resonance fluorescence imaging in non-intrusive cargo inspection," Nucl. Instr. Meth. Phys. Res. B 241 (2005) pp. 820-825.
[2] J. Pruet et al., "Detecting clandestine material with nuclear resonance fluorescence," J. App. Phys. 99, 123102 (2006).
[3] B.J. Quiter, B.A. Ludewigt, V.V. Mozin, S.J. Tobin, "Nondestructive Spent Fuel Assay Using Nuclear Resonance Fluorescence," *Annual Meeting of the Institute of Nuclear Material Management*, Tucson, AZ, 2009.
[4] B.A. Ludewigt, V.V. Mozin, A.H. Haefner and B.J. Quiter, "Using Nuclear Resonance Fluorescence for Nondestructive Isotopic Analysis," Inst. of Nucl. Mat. Man., 51st Ann. Mtg., Baltimore, MD, July 11-15 (2010).
[5] B.J. Quiter, B.A. Ludewigt and S.D. Ambers, "Assesment of Nuclear Resonance Fluorescence for Spent Nuclear Fuel Assay," Inst. of Nucl. Mat. Man., 52st Ann. Mtg., Palm Desert, CA, July 17-21 (2011).
[6] C.G.R. Geddes, E. Cormier-Michel, E.H. Esarey, C.B. Schroeder, J-L. Vay, W.P. Leemans, and the LOASIS team, LBNL; D.L. Bruhwiler, J.R. Cary, B. Cowan, M. Durant, P. Hamill, P. Messmer, P. Mullowney, C. Nieter, K. Paul, S. Shasharina, S. Veitzer, and the VORPAL development team, Tech-X; G. Weber, O. Rubel, D. Ushizima, Prabhat, and E.W. Bethel, VACET; and J. Wu, SciDAC Scientific Data Management Center, "Laser Plasma Particle Accelerators: Large Fields for Smaller Facility Sources," SciDAC Review 13, pp. 13 (2009). LBNL-2299E.
[7] F. Albert et al., "Precision linac and laser technologies for nuclear photonics gamma-ray sources," Phys. of Plamas 19, 056701 (2012).
[8] J. Hall et al., "Numerical simulation of nuclaer materials detection, imaging and assay with MEGa-rays," Inst. of Nucl. Mat. Man., 52st Ann. Mtg., Palm Desert, CA, July 17-21 (2011) LLNL-CONF-485911.
[9] B.J. Quiter, T. Laplace, B.A. Ludewigt, S.D. Ambers, B.L. Goldblum, S. Korbly, C. Hicks, C. Wilson, "Nuclear resonance fluorescence in ^{240}Pu," *Submitted to Phys. Rev. C* (2012).
[10] R.D. Heil, H.H. Pitz, U.E.P Berg, U. Kneissl, K.D. Hummel, G. Kilgus, D. Bohle, A. Richter, C. Wesselborg, and P. Von Brentano, "Observation of orbital magnetic dipole strength in the actinide nuclei ^{232}Th and ^{238}U." Nuc. Phys. A476 (1988), pp. 39-47
[11] W. Bertozzi, J.A. Caggiano, W.K. Hensley, M.S. Johnson, S.E. Korbly, R.J. Ledoux, D.P. McNabb, E.B. Norman, W.H. Park, and G.A. Warren, "Nuclear resonance fluorescence excitations near 2 MeV in ^{235}U and ^{239}Pu," Phys. Rev. C 041601(R) (2008).
[12] J.F. Pelowitz (ed.), "MCNPX^{TM} USERS MANUAL Version 2.6.0," LA-CP-07-1473 (2008).
[13] Gregg W. McKinney, Alex B. McKinney, John S. Hendricks, Denise B. Pelowitz, and Brian J. Quiter, "MCNPX NRF LIBRARY - RELEASE 2," *ANS Annual Meeting*, San Diego, CA, June 2010.
[14] M.R. James, G.W. McKinney, J.W. Durkee, M.L. Fensin, J.S. Hendricks, D.B. Pelowitz, R.C. Johns, L.S. Waters, J.S. Elson, M.W. Johnson, B. Quiter, "Implementation of Homeland Security Features in MCNP/X," *IEEE NSS*, Oct. 31-Nov. 6, 2010, Knoxville, TN, LA-UR-10-07256.
[15] John S. Hendricks and Brian J. Quiter, "MCNP/X Form Factor Upgrade for Improved Photon Transport," (LA-UR-10-01096) *Journal of Nuclear Technology*, p. 150, Vol. 175, July 2011.
[16] B.J. Quiter, B.A. Ludewigt, V.V. Mozin, C. Wilson, and S. Korbly, "Transmission Nuclear Resonance Fluorescence Measurement of ^{238}U," Nucl. Inst. Meth. Phys. Res. B 269 (2011) pp. 1130-1139.